Defence Science Journal, Vol. 51, No. 4, October 2001, pp. 419-427

Short-term Settlement of Footing on Snow Foundation

Puneet Mahajan

Indian Institute of Technology, New Delhi–110 016

ABSTRACT

A constitutive theory for snow, developed by the authors, is applied to solve for the short-term settlement of footing on snow foundation. The constitutive law used is a microstructurally-based formulation which includes the effects of bond deformation and fracture. It also includes transient creep effects and strain hardening of snow. The foundation problem is solved for stress and displacement distribution, with two different loads of 0.008 MPa and 0.1 MPa distributed uniformly over a part of the top face. The stress distribution matches closely with the existing theoretical results.

Keywords: Constitutive theory of snow, transient creep effects, bond deformation and fracture, strain hardening of snow

1. CONSTITUTIVE THEORY

Snow existing under equitemperature conditions is made of spherical ice grains connected by bonds or necks. The constitutive behaviour of snow is determined by the size of the ice particles and the geometry of bonds connecting the grains. Because of their smaller cross-section, the bonds or the necks are subjected to much higher stresses when compared to the ice particles, and therefore undergo large deformations. It is the straining of necks which is responsible for deformation of snow, particularly at low stresses. At higher stresses, the necks undergo fracture, and interparticle slip becomes a significant deformation mechanism. It is this relative displacement between the particles responsible for strains in snow at large stresses. At these stresses, snow behaves somewhat like other granular materials. The deformation of snow is therefore an averaged effect of the deformation of the unbroken necks and of relative sliding between particles with broken necks.

A constitutive theory taking into account these deformation mechanisms, has been suggested by Mahajan and Brown[1]. In this theory, the stresses at the points of contact of a representative particle are calculated using the variational approach suggested by Kanatani[2]. Next, the strains in the necks are calculated using equations developed for constitutive behaviour of ice. If fracturing of necks takes place, empirical relations are developed to model the strains at the contact points, due to the relative sliding between ice particles. The strains are then averaged, over the representative particle, to obtain the strains in snow.

Consider a typical ice grain and the necks or bonds which connect it to other grains. To calculate the stresses in the necks, a local coordinate system, as illustrated in Fig. 1, is setup at the contact point. The stress vector at the contact point or the ice neck is resolved into three components along the coordinate axis of this local coordinate system. The unit vectors for this coordinate system are:

Revised 18 October 2000

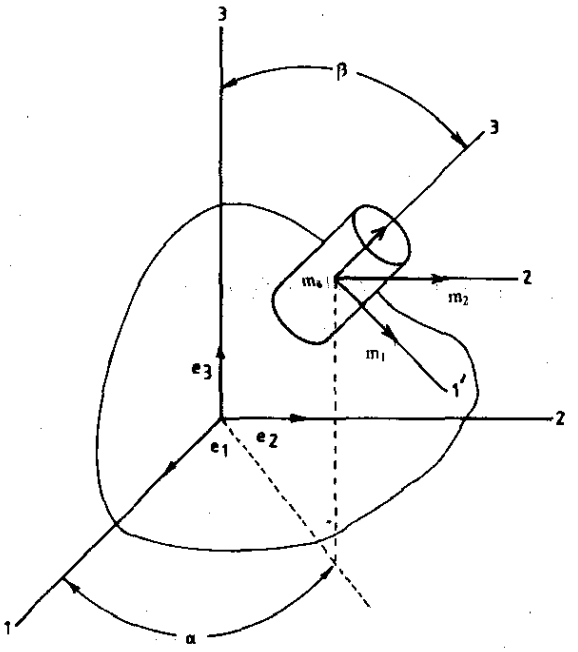

Figure 1. Coordinate system: 1-2-3 global coordinate system centred at ice particle centre. 1'-2'-3' neck coordinate system centred at the centre of neck.

$$\left.\begin{aligned} m_1 &= \cos\alpha\cos\beta\, e_1 + \sin\alpha\sin\beta\, e_2 - \sin\beta\, e_3 \\ m_2 &= -\sin\alpha\, e_1 + \cos\alpha\, e_2 \\ m_3 &= \cos\alpha\sin\beta\, e_1 + \sin\alpha\cos\beta\, e_2 + \cos\beta\, e_3 \end{aligned}\right\} \quad (1)$$

The stress vector in the necks, on the face with normal n, is given by

$$\sigma^n A_T P = \frac{a^2}{\gamma} t^n \quad (2)$$

where σ^n is the traction vector on the bond. A_T is the contact area, P is the probability of contact, γ the density ratio defined as density of ice/density of snow, a is the particle size and t^n is the traction vector on snow.

The vector n is same vector as m_3 in Eqn (1) above. The components of stress on the face with normal n are given as

$$\sigma_{i3} = m_i.\sigma^n \quad (3)$$

If averaging is done over the area of contact lying between the solid angle imbedded by angles α to $\alpha + \Delta\alpha$ and β to $\beta + \Delta\beta$, one obtains:

$$(\sigma_{i3})_{av} = \frac{\int_{\beta}^{\beta+\Delta\beta}\int_{\alpha}^{\alpha+\Delta\alpha} t^n.m_i \frac{a^2}{\gamma}\sin\beta\, d\alpha\, d\beta}{\int_{\beta}^{\beta+\Delta\beta}\int_{\alpha}^{\alpha+\Delta\alpha} A_T.P\sin\beta\, d\alpha\, d\beta}$$

The strain rates in the necks are based on the theory developed by Szyszkowski and Glockner[3] and are given by the following relations:

$$\dot{e}_{ij} = \frac{(1+\nu)}{E}\dot{\sigma}_{ij} - \frac{\nu}{E}\dot{\sigma}_{kk}\delta_{ij} + \frac{1}{\nu_1}\frac{d}{dt} \int_0^t \left[\tilde{\sigma}_{ij}(\tau)\right]^n j(t-\tau)d\tau \frac{\tilde{\sigma}_{ij}}{\nu_2} \quad (4)$$

where

$$\tilde{\sigma}_{ij} = s_{ij}\left\{1.5\left|\frac{S}{s_{ij}}\right|^{n-1}\right\}^{1/n} \quad (5)$$

$$S^2 = 1.5 s_{ij} s_{ij}$$

In Eqn (4) ν is the Poisson's ratio; E is the Young's modulus, j is the creep compliance, and ν_1 and ν_2 are constants. The s_{ij} is the deviatoric stress. The strain rate is decomposed into elastic, recoverable creep and plastic components.

$$\dot{e}_{ij} = \dot{e}^e_{ij} + \dot{e}^c_{ij} + \dot{e}^p_{ij} \quad (6)$$

The expressions for various components as observed from Eqn (4) are:

$$\dot{e}^e_{ij} = \frac{(1+\nu)}{E}\dot{\sigma}_{ij} - \frac{\nu}{E}\dot{\sigma}_{kk}\delta_{ij} \quad (7)$$

$$\dot{e}^c_{ij} = \frac{1}{\nu_1}\frac{d}{dt}\int_0^t \left[\tilde{\sigma}_{ij}(\tau)\right]^n j(t-\tau)d\tau \quad (8)$$

$$\dot{e}^p_{ij} = \frac{\tilde{\sigma}^n_{ij}}{\nu_2} \quad (9)$$

Instead of directly solving the integral in Eqn (8), Szyszkowski and Glockner[3] have approximated Eqns (8) and (9) by a generalised Kelvin body in series with a nonlinear dashpot. The equations for the Kelvin body are written as

$$\dot{e}_{ij}^{c} = \frac{(\tilde{\sigma}_{ij''})^n}{\nu_2} \tag{10}$$

$$(\tilde{\sigma}'_{ij''})^n + c\tilde{\sigma}'_{ij}(\tilde{\sigma}'_{ij})^{n-1} = E_1 e_{ij}^{c} \text{ (no summation)} \tag{11}$$

$$\tilde{\sigma}'_{ij} + \tilde{\sigma}''_{ij} = \tilde{\sigma}_{ij} \tag{12}$$

where $\tilde{\sigma}_{ij}$ is the effective viscous stress tensor defined above, $\tilde{\sigma}'_{ij}$ is the component of effective stress in the spring and $\tilde{\sigma}''_{ij}$ is the component of effective stress in the dashpot. The value of the constants ν_1 and ν_2 depends on the stress in the necks. If the principal tensile stress in the neck is < 0.7 MPa, the constants ν_1 and ν_2 have values of 10.8 and 235, respectively. Otherwise, ν_2 is equal to 5040. The values of the constants for two cases are different because the deforming mechanisms, as explained by Boyce and Spence[4], are different. For principal stress in necks is ≤ 0.7 MPa, superplastic deformation occurs whereas for stress higher than this, dislocation creep becomes predominant.

The strains in the ice necks are next transformed to the snow coordinate system by the equation:

$$E_{ij} = Q_{ir}^{T} e_{rs} Q_{si} \tag{13}$$

where Q is an orthogonal transformation matrix carrying the local coordinate system centred at the neck to the global coordinate system centred at ice particle centre (Fig. 1).

If the principal stress in necks is > 0.7 MPa and principal strain exceeds 5×10^{-3}, it is assumed that the neck has lost the ability to carry principal tensile stress, and therefore fractures. After the occurrence of fracture, deformations in snow are due to interparticle sliding.

The tangential and normal velocities and displacements are calculated using the equation

$$\dot{\eta} = c_1(tau)|tau|^{n-1}\left(\frac{1}{disp^m}\right) \tag{14}$$

$$\dot{\xi} = c_1(tnor)|tnor|^{n-1}\left(\frac{1}{disp^m}\right)c_2 \tag{15}$$

where $\dot{\xi}$ and *tnor* are the velocity and the component of traction in the direction normal to the grain surface at the neck, respectively. The $\dot{\eta}$ is the tangential velocity, *tau* is the component of traction in the shearing direction, and *disp* is the relative displacement between the grains at a particular time. The expression $1/disp^m$ appears because as the sliding displacement increases, the particles form new contacts with other particles and this impedes further relative displacement. This seems to account for much of the strain hardening in snow. The parameter m was obtained, using regression fit, as a function of effective strain in snow. The constant c_1, in Eqns (14) and (15), has a value of 3.906×10^{-3}. The constant c_2 depends on the ratio of shear to compressive stress at the point of contact. If the absolute value of the ratio of shear to compressive stress is < 0.5, then c_2 is equal to 0.3. Otherwise, it has a value of 0.40. The constant n has a value of 1.8. The parameters c_1, c_2 and m have slightly different values for tensile stress states. For tension c_1 is 5.468×10^{-3} and c_2 is approx. 0.1. The strain rate is given by the expression:

$$\dot{E}_{ij} = \frac{1}{a}\left(\frac{1}{2}\dot{\eta}(s_i n_j + s_j n_i) + \dot{\xi} n_i n_j\right) \tag{16}$$

The strain in snow is the average of strain in all necks.

$$(E_{ij})_{av} \int_0^{2\pi}\int_0^{\pi} \sin\beta \, d\alpha d\beta = \int_0^{2\pi}\int_0^{\pi} E_{ij} \sin\beta \, d\alpha d\beta \tag{17}$$

where $E_{ij}\sin\beta d\alpha d\beta$ on the right hand side is obtained from Eqn (13) or Eqn (17), depending on

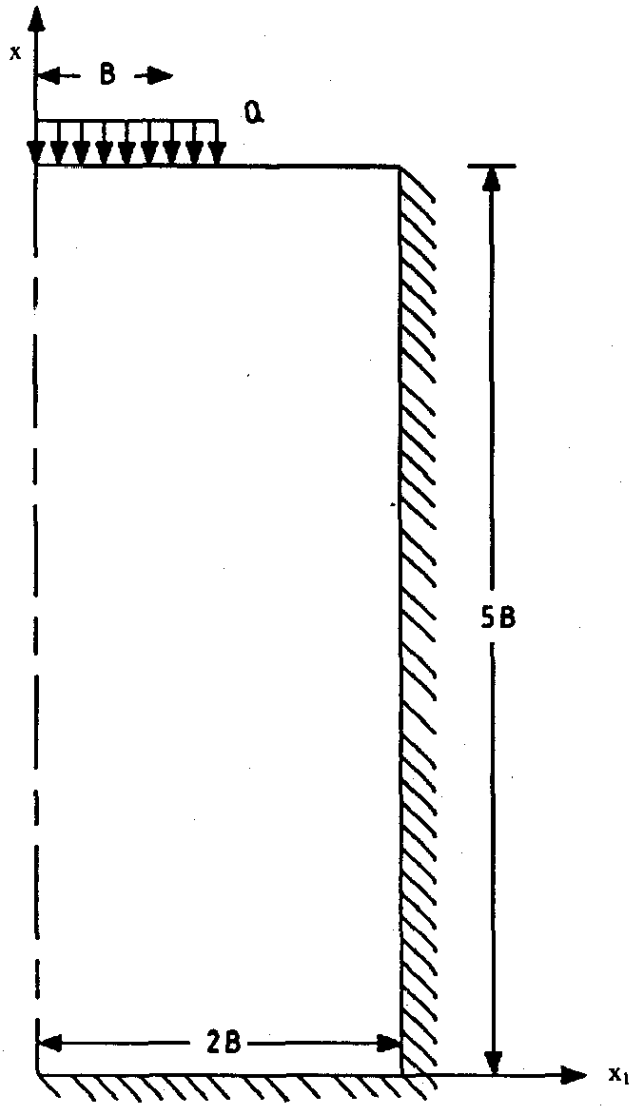

Figure 2. Foundation with stress of Q MPa (B = 0.45 m). Symmetry wrt x_1 allows only half-of- foundation and snowcover region to be analysed.

whether it is a broken neck or a neck undergoing superplastic deformation. The $(E_{ij})_{av}$ is the strain in snow averaged over the solid angle.

2. NUMERICAL SOLUTION

It has been experimentally observed that for symmetrical loading, the vertical and horizontal extent of the deformation zone (pressure bulb) in a foundation extends to about two times the width of the footing[5]. For simplicity, a rectangular area underneath the footing is considered as shown in Fig. 2. The dimensions of this rectangle are larger than the observed size of the pressure bulb.

Plane strain has been assumed for this problem, and therefore, a 3-D state of stress exists. The method followed in solving these problems is a commonly used technique involving creep of structures. This method is closely linked to the elastic solution procedure. This relation between creep and elastic solutions derives from the fact that, after initial loading, creep strains arising during the passage of time require that stresses change by elastic straining to accommodate these changes[4].

The stress strain relation for isotropic elastic material is:

$$\sigma_{ij} = \lambda e^e_{kk} + 2\mu e^e_{ij}$$

where λ and μ are Lame's constants. This last relation can be written as .

$$\sigma_{ij} = \lambda(e_{kk} - e^c_{kk})\delta_{ij} + 2\mu(e_{ij} - e^c_{ij})$$

$$\sigma_{ij} = \lambda\left(\frac{\partial u_k}{\partial x_k} - e^c_{kk}\right)\delta_{ij} + \mu\left(\frac{\partial u_i}{\partial x_j} + \frac{\partial u_j}{\partial x_i} - 2e^c_{ij}\right) \qquad (18)$$

Substituting this into the equilibrium equation, one gets:

$$\mu(\Delta^2 u_j) + (\lambda + \mu)\Delta_j \Delta_i u_i + \rho b_j = \lambda \frac{\partial e^c_{kk}}{\partial x_j} + 2\mu \frac{\partial e^c_{ij}}{\partial x_i} \qquad (19)$$

For the case of plane strain, the reduced Navier's equations are:

$$G\left[\Delta^2 u_1 + \frac{1}{2v}\frac{\partial}{\partial x_1}\left(\frac{\partial u_1}{\partial x_1} + \frac{\partial u_2}{\partial x_2}\right) + \rho b_1\right] = \frac{Ev}{(1+v)(1-2v)}$$

$$\left(\frac{\partial e^c_{11}}{\partial x_1} + \frac{\partial e^c_{22}}{\partial x_1} + \frac{\partial e^c_{33}}{\partial x_1}\right) + 2G\left(\frac{\partial e^c_{11}}{\partial x_1} + \frac{\partial e^c_{21}}{\partial x_2}\right) \qquad (20)$$

$$G\left[\Delta^2 u_2) + \frac{1}{1-2v}\frac{\partial}{\partial x_2}\left(\frac{\partial u_1}{\partial x_1} + \frac{\partial u_2}{\partial x_2}\right) + \rho b_2\right] = \frac{Ev}{(1+v)(1-2v)}$$

$$\left(\frac{\partial e^c_{11}}{\partial x_2} + \frac{\partial e^c_{22}}{\partial x_2} + \frac{\partial e^c_{33}}{\partial x_2}\right) + 2G\left(\frac{\partial e^c_{22}}{\partial x_2} + \frac{\partial e^c_{12}}{\partial x_1}\right) \qquad (21)$$

The boundary conditions are:

Top face:

$$x_2 = 2.25 \text{ m } Q = Q_0 \quad 0 \le x_1 \le 0.45 \text{ m}$$

$$Q = 0 \quad x_1 > 0.45 \text{ m}$$

$$T_{xy} = 0 \quad 0 \le x_1 \le 0.9 \text{ m}$$

Using the above relations in the constitutive relations (Eqn (18)), one gets:

$$Q=(\lambda+2\mu)\left(\frac{\partial u_2}{\partial x_2}-e_{22}^c\right)+\lambda\left(\frac{\partial u_1}{\partial x_1}-e_{11}^c\right)-\lambda_{33}^c \quad (22)$$

$$\left(\frac{\partial u_2}{\partial x_1}+\frac{\partial u_1}{\partial x_2}\right)=2e_{12}^c \quad (23)$$

Axis of symmetry:

$$\frac{\partial u_2}{\partial x_1}=0,\ u_1=0 \qquad 0\le x_1\le 0.9\text{m}, x_2=0 \quad (24)$$

Bottom and right vertical side:

$$u_1 = 0,\ u_2 = 0 \qquad 0\le x_1\le 0.9\text{m}, x_2=0$$

and

$$x_1=0.9\text{m}, \qquad 0\le x_2\le 2.25\text{m} \quad (25)$$

If the boundary conditions for the top face are substituted into Eqns (20) and (21), one obtains:

$$G\left[\left(1+\frac{1}{(1-2v)}\right)\frac{\partial^2 u_1}{\partial x_1^2}+\left(1+\frac{1}{(1-2v)}\right)\frac{\partial^2 u_2}{\partial x_2^2}\right] = \frac{Ev}{(1+v)(1-2v)}\left(\frac{\partial e_{11}^c}{\partial x_1}+\frac{\partial e_{22}^c}{\partial x_1}+\frac{\partial e_{33}^c}{\partial x_1}\right) + 2G\left(\frac{\partial e_{21}^c}{\partial x_1}+\frac{\partial e_{11}^c}{\partial x_2}\right)-\frac{2}{(1-2v)}\frac{\partial e_{12}^c}{\partial x_2} \quad (26)$$

$$G\left[\left(1+\frac{1}{(1-2v)}\right)\frac{\partial^2 u_2}{\partial x_2^2}+\left(1-\frac{1}{(1-2v)}\right)\frac{\partial^2 u_1}{\partial x_1^2}\right]+\rho b_2 = \frac{Ev}{(1+v)(1-2v)}\left(\frac{\partial e_{11}^c}{\partial x_2}+\frac{\partial e_{22}^c}{\partial x_2}+\frac{\partial e_{33}^c}{\partial x_2}\right) + 2G\left(\frac{\partial e_{22}^c}{\partial x_2}+\frac{\partial e_{12}^c}{\partial x_1}\right)-\frac{2}{(1-2v)}\frac{\partial e_{21}^c}{\partial x_1} \quad (27)$$

The symmetry boundary condition, in substitution into the Eqn (20), acquires the form

$$G\left[\left(1+\frac{1}{(1-2v)}\right)\frac{\partial^2 u_2}{\partial x_2^2}+\frac{\partial^2 u_1}{\partial x_1^2}\right]+\rho b_2 = \frac{Ev}{(1+v)(1-2v)}\left(\frac{\partial e_{11}^c}{\partial x_2}+\frac{\partial e_{22}^c}{\partial x_2}+\frac{\partial e_{33}^c}{\partial x_2}\right)+2G\left(\frac{\partial e_{22}^c}{\partial x_2}+\frac{\partial e_{12}^c}{\partial x_1}\right)$$

It has been assumed that all the necks fracture after a certain time. The above differential equations with boundary conditions are solved using the finite deference method. Central finite differences have been used throughout. A grid with mesh refinement near the top face has been used. The problem was solved for two different values of Q_0, namely 0.008 MPa and 0.1 MPa.

Although not obvious, these equations are time dependent. The time dependence appears because the creep strains in the above equations change with time. The first step in solving these equations involves finding the elastic solution at time $t = 0$. For this the creep terms on the right hand side are set to zero. The stresses from this elastic solution are then used to calculate the creep strain rates using equations. Once the creep strains have been calculated from these creep rate equations, these are substituted in the above differential equations, which are solved for displacements at end of time step. The new stresses at the end of time step are next calculated. Due to the rather complex nature of creep equations, it is not possible to use implicit method to integrate the creep strain rate equations and the explicit methods have been used, posses a big limitation on the size of the time step. The grain data reported by Hansen was used. For

a compressive stress of 8×10^{-3} MPa with a time step of 120 s, a steadystate of stress is not reached even after 300 iterations, although the rate of change of stress does exhibit a decreasing trend. For instance, the rate of change of the largest stress decreases from 1.5×10^{-4} MPa/hr at the beginning to 3×10^{-5} MPa/hr by the 300th iteration. Since this rate of change is small, it was decided to assume a steadystate of stress after 3000 time steps.

For Q equal to 0.1 MPa, there are areas under the loading where stresses are high enough to cause the neck fracturing after a very small period of time. On the other hand, there are areas away from the loading region at which the stresses are low enough that according to the theory developed, superplastic deformation should be taking place in necks. At the boundary of these two areas, there are regions where ice necks, at a particular solid angle, have a principal stress of, eg, 0.7 MPa at one grid point, and at the next grid point the principal neck stress, for the same solid angle, is 0.705 MPa. In the theory it has been assumed that for stresses $\leq$ 0.7 MPa superplastic deformation takes place, whereas for stresses greater than this value, deformation is due to sliding of particles. Therefore at the first grid point the neck is undergoing a superplastic deformation, whereas at the second grid point there is relatice sliding between the particles. This results in discontinuous strain rates (because the strain rates for superplastic deformation and sliding are different) and also leads to a situation where regions of low stress have higher strain rates as compared to regions with higher stress (superplastic strain rate at 0.7 MPa is higher than sliding rate at the same stress). To avoid this discontinuity in strain rates, it was assumed that necks remain intact for the first 50 iterations, deforming according to the creep law for high stresses. After 50 iterations, all necks were assumed to have broken, and relative sliding of particles was taken as the sole deforming mechanics for the whole problem. The solution becomes unstable rather quickly if this assumption is not made.

At this load it was found that with a time step of 120 s the stresses continue to decrease, as was expected, for 150 iterations. However, after that the high stresses change negligibly, but the low stresses, instead of decreasing, begin increasing and the problem becomes unstable, as indicated by large changes in lateral stresses and a decrease in vertical displacement instead of an increase. It is possible that by use of a still smaller time step this problem can be remedied, but this would also result in an increased computational time. This instability seems to be associated with the strain hardening in that constitutive equation becoming significant. Most multiaxial creep problems are solved using implicit method, and even then a very short time step has to be used. So the instability with the use of the explicit method for strain hardening problem is not surprising. It was decided to take the stresses at the end of 150 iterations as the stresses to be used for all future iterations. By imposing this restriction, the equilibrium equation is being violated. However, the change in maximum stresses by the 150th iteration are small and this assumption was considered to be reasonable.

For low compressive stress of 8×10^{-3} MPa, the normalised vertical stress component [stress/

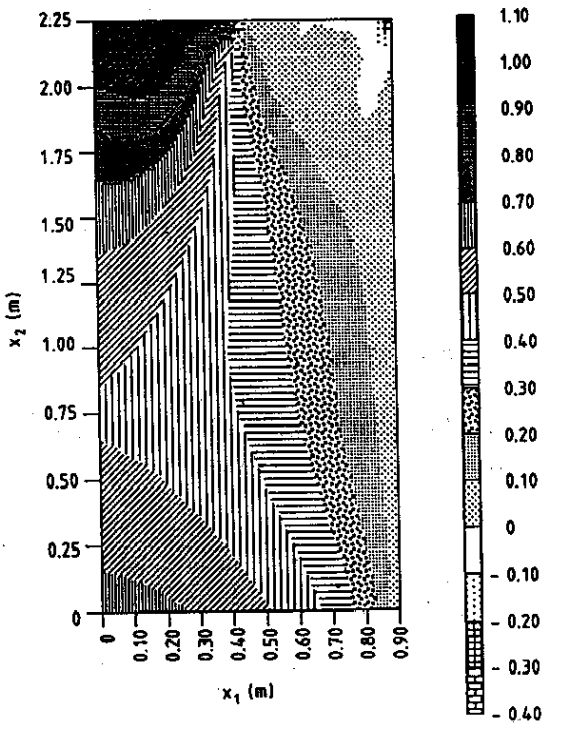

Figure 3. Normalised stress contours by 7 hr for Q = 0.008 MPa. The stress were assumed to have reached a steady value at this time.

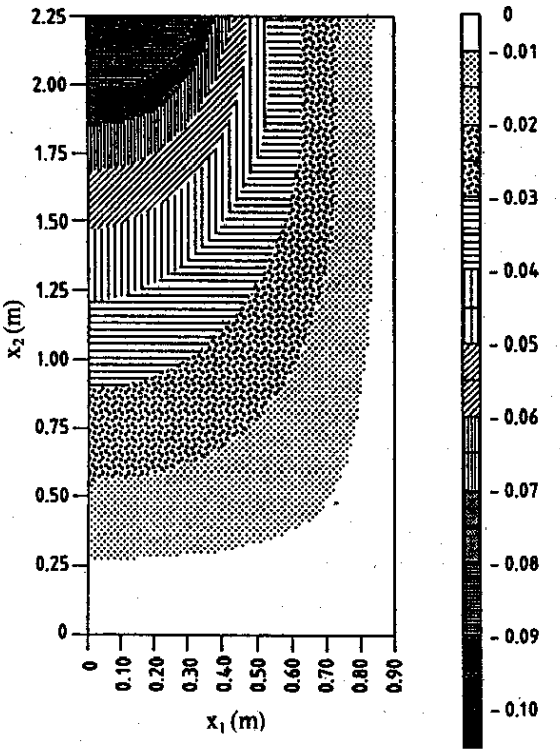

Figure 4. Displacement contours by 60 hr (Q = 0.008 MPa)

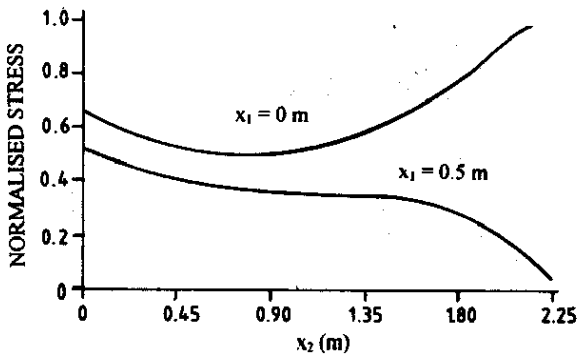

Figure 5. Stress distribution along vertical section at centreline and 0.5 m from centreline (Q = 0.008 MPa).

$(8 \times 10^{-3}$ MPa)] contours are shown in Fig. 3 and the displacement contours at the end of 60 hr are shown in Fig. 4. A steadystate of stress was assumed to have been reached by 7 hr. From these, it becomes apparent that the stresses are much higher closer to the axis of symmetry and fall to a very low value as one moves away from this axis of symmetry and fall to a very low value as one moves away from this axis. Also, the stresses beneath the loaded area at 0.45 m from the bottom are about 65 per cent of the stresses at 0.45 m from top. Figure 5 illustrates the stress distribution along two vertical sections. For a section at the axis of symmetry, the stresses first decrease with height and then rise. The stresses are high at the bottom because the body force effect is almost half the value of applied stress. Had the body forces not been taken into account, the stress at the bottom would have been much lower than that stress at the top. At the section 0.5 m from the axis of symmetry, Q = 0. Here, the stress at the bottom is only about 25 per cent lower than that at a section along axis of symmetry, probably because the stresses here again are largely due to weight of snow. From Fig. 4, it is seen that vertical displacements are the highest right under the applied load. At the end of 60 hr the maximum vertical displacement is 0.1 cm. The maximum horizontal displacement is about 0.25 times more than this value.

For Q equal to 0.1 MPa, the body forces are insignificant compared to the external load. The

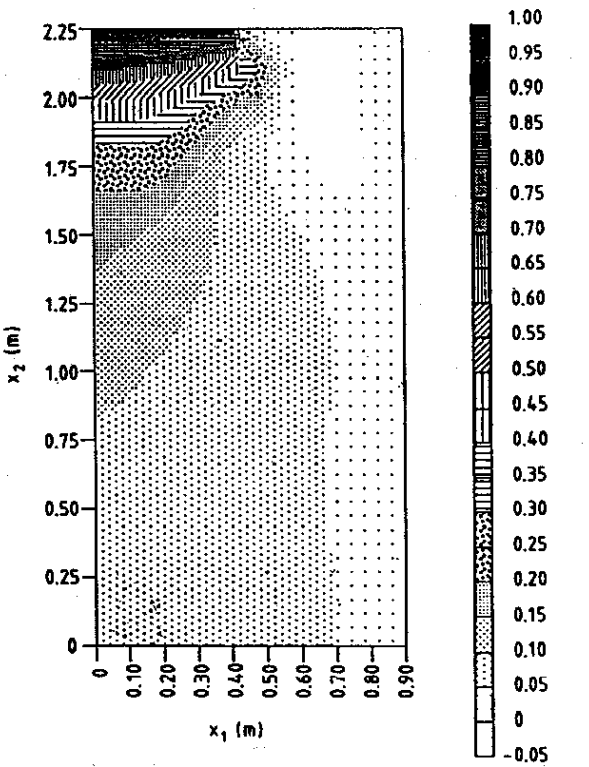

Figure 6. Normalised stress contours by 5 hr for Q = 0.1 MPa. The stresses were assumed to have reached a steady value at this time.

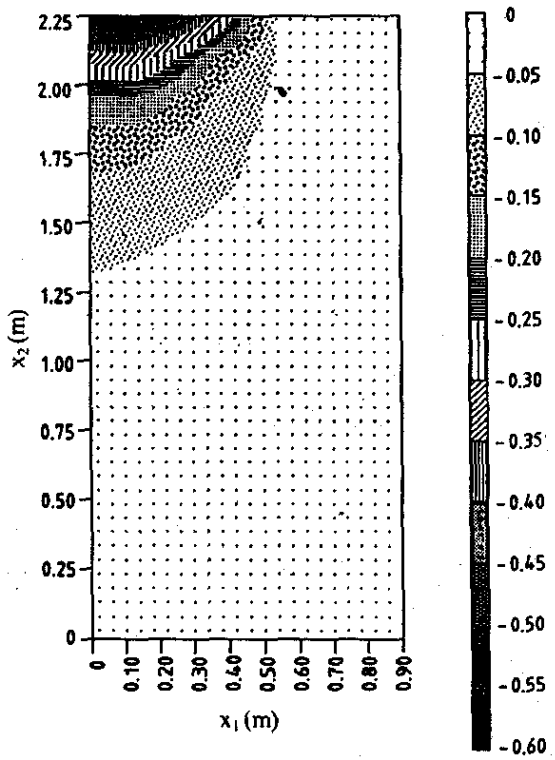

Figure 7. Displacement contours by 30 hr (Q = 0.1 MPa)

normalised stress contours and displacement contours are shown in Figs 6 and 7, respectively. The stress in the section right under the footing shows a big drop within the top 0.50 m, the stresses at 1.6 m are 20 per cent of the value at the top. This is consistent with experimental data according to which the pressure bulb extends to about two times the width of the footing. Body forces being insignificant compared to load, the stresses at the bottom are < 10 per cent of the values at the top. This is in sharp contrast

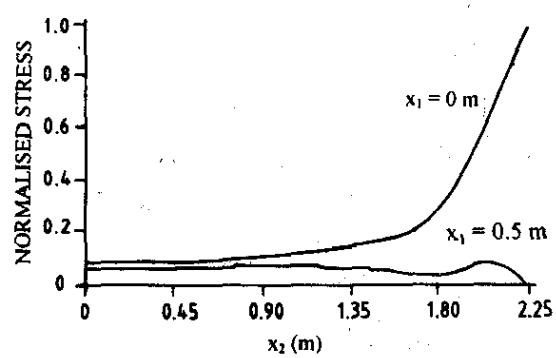

Figure 8. Stress distribution along vertical section at centreline and 0.5 m from centreline (Q = 0.1 MPa).

to values at the bottom for $Q = 8 \times 10^{-3}$ MPa, which were almost 75 per cent of the values at the top. Figure 8 shows the stress distribution at a section 0.45 m from axis of symmetry. This shows a fairly constant value for stresses from top to bottom. The displacement contours in Fig. 8 shows that major displacements are largely restricted to about the top 0.9 m of the foundation. The gradients in vertical displacement were more gradual for 8×10^{-3} MPa, than for 0.1 MPa. The maximum displacement at the end of 30 hr was 0.57 cm.

CONCLUSION

In this paper, a constitutive theory developed earlier has been applied to solve the settlement of foundation subject to a uniformly distributed load on a part of its top surface. The constitutive theory is based on the microstructure and various constants used have not to be changed when the grain size or bond size changes. The theory is also able to model strain hardening in snow due to increase in the 3-D coordination number with increase in strains. However, no attempt has been made to model strain hardening due to metamorphic processes which are active during deformation. Since, the short duration deformation are considered, the later may not be important.

Presently, there is not much data available for comparison with the example given here. The data presented by Reed[5] and used by Dandekar and Brown[6] for comparison of their results is for long-term settlement of foundation. The general behaviour of Dandekar's result was in agreement with the data presented by Reed. The stress distribution determined with the theory presented here matches closely to that presented by Dandekar and Brown[6].

The present theory suffers from drawbacks of excessive computational time and instability of solution once strain hardening becomes significant. This problem may be remedied, as has been suggested by Mahajan and Brown, by the use of invariant theory. The data required for determining the various constants in the invariant theory can be obtained from the present theory.

REFERENCES

1. Mahajan, P. & Brown, R.L. A microstructure-based constitutive law for snow. *Annals of Glaciology*, 1993, **17**, 287-94.
2. Kanatani, K. A theory of contact force distribution in granular material. *Powder Technology*, 1981, **28**, 4.
3. Szyszkowski, W. & Glockner, P. G. Modelling the mechanical properties of ice. *In* Proc. of Sixth International Offshore Mechanics and Arctic Engineering Symposium, ASME, 1987.
4. Boyle, J.T. & Spence, J. Stress Analysis for Creep, Butterworths, 1983.
5. Reed, Sherwood, C. Spread footing foundations on snow. CRREL Report-TR1–75.
6. Dandekar, B.W. & Brown, R.L. A numerical evaluation of flexible footing into uniform snow cover. *Cold Regions Sci. Technol.*, 1986, **12**, 131-38.

Contributor

Dr Puneet Mahajan obtained his PhD in Mechanical Engineering. Presently, he is working as Associate Professor in the Dept of Applied Mechanics at the Indian Institute of Technology, New Delhi. His research interests include: Low velocity impact of composites, vibrations, snow mechanics and application of finite element method to above areas.